White matter tauopathy: transient functional loss and novel myelin remodeling.

Running title: White matter tauopathy

Joshua Jackson[1], Gabby Bianco[1], Angelo O Rosa[2], Katrina Cowan[3,] Peter Bond[2], Oleg Anichtchik[3], and Robert Fern[3].*

[1] University of Bath, UK.
[2] Plymouth Electron Microscopy Centre, University of Plymouth, UK.
[3] University of Plymouth, PUPSMD, Plymouth, UK

*To whom correspondence should be addressed: Peninsula Schools of Medicine and Dentistry, University of Plymouth, John Bull Building, Research Way, Plymouth, PL6 8BU, UK. Robert.fern@plymouth.ac.uk

Word count: Abstract, 250; Introduction, 489; Materials and Methods, 943; Results, 1650; Discussion, 1258.

Acknowledgments: We thank Waldemar Woznica for assistance with animal care. This work was supported by BBSRC (J016969/1), Alzheimer's Research UK (South-West network centre grant), and by the University of Plymouth.

Table of contents image:

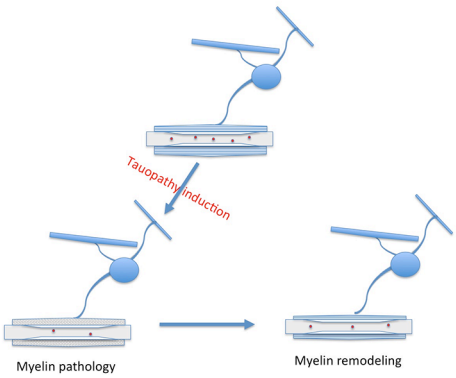

Main points:

- Mutant tau induction produced myelin pathology within weeks associated with failure of action potential conduction.
- Myelin remodeling accompanied continued transgene induction, producing a thin myelin phenotype with restored excitability.

Abstract

Early white matter (WM) changes are common in dementia and may contribute to functional decline. We here examine this phenomenon in an induced dementia model for the first time. We report a novel and selective form of myelin injury as the first manifestation of tauopathy in the adult CNS. Myelin pathology rapidly followed the induction of a P301 tau mutation associated with fronto-temporal dementia in humans (rTG4510 line). Damage involved focal disruption of the ad-axonal myelin lamella and internal oligodendrocyte tongue process, followed by myelin remolding with features of re-myelination that included myelin thinning and internodal shortening. The evolution of the re-myelinated phenotype was complete in the molecular layer of the dentate gyrus (ML DG) after 1 month and in the optic nerve (ON) after 9 months of transgene induction and proceeded in the absence of actual demyelination, reactive glial changes or inflammatory response. The initial rapid myelin pathology was associated with loss of WM function and performance decline in a novel recognition test and both these effects largely reversed during the myelin re-modeling phase. The initial phase of myelin injury was accompanied by disruption of the vesicle population present in the axoplasm of hippocampal and ON axons. Axoplasmic vesicle release is significant for the regulation of myelin plasticity and disruption of this pathway may underlie the myelin damage and remodeling evoked by tauopathy. WM dysfunction early in tauopathy will disorder neural circuits, the current findings suggest this event may make a significant contribution to early clinical deficit in dementia.

Key words: Axon; Dementia; Myelin; Oligodendrocyte; White matter

Introduction

Hyper-phosphorylated and misaggregated forms of the microtubule-associated protein tau (MAPT) are present in various forms of dementia and are implicated in disease pathogenesis (Goedert & Spillantini, 2006; Zempel & Mandelkow, 2014) (Boeve & Hutton, 2008). In the healthy CNS, tau is enriched in WM brain structures and localizes to the axonal projections of neurons where it plays a role in microtubule stability (Binder, Frankfurter, & Rebhun, 1985; Harada et al., 1994; Zempel & Mandelkow, 2014). In dementias such as Alzheimer's disease (AD) and fronto-temporal dementia (FTD), tau is miss-sorted to the soma/dendrites and can aggregate to form neurofibriliary tangles and threads. The majority of central axons are located in WM and WM structural changes are a common feature of dementia. For example, histological, imaging and biomarker studies report WM involvement in ~60% of AD cases (Brun & Englund, 1986; de la Monte, 1989; Roher et al., 2002; Schmahmann, Smith, Eichler, & Filley, 2008; Skillback, Zetterberg, Blennow, & Mattsson, 2013; Yin et al., 2015). WM changes in dementia were originally considered to be secondary to the pathological progression of gray matter elements such as synapses and neuronal somata, but this is inconsistent with the timing of events. WM structural changes are some of the earliest indications in brain imaging studies of AD (Amlien & Fjell, 2014; Back et al., 2011; Brun & Englund, 1986; de la Monte, 1989; Gold, Johnson, Powell, & Smith, 2012; Schmahmann et al., 2008), and prodromal forms of AD are associated with an elevation in WM injury biomarkers and the presence of structural changes indicative of myelin pathology (Amlien & Fjell, 2014; Skillback et al., 2013; Zetterberg et al., 2015; B. Zhang, Xu, Zhu, & Kantarci, 2014). Microstructural WM changes are also apparent years before the onset of symptoms in sporadic AD of genetic origin (Bendlin et al., 2010; Gold et al., 2012).

It is well established that neurological decline in dementia is accompanied by the disruption of neural networks, while axonal projections maintained by WM underpin all networks connections in the CNS (Brier et al., 2012; Provenzano et al., 2013; Teipel et al., 2016). Any compromise of WM function associated with the early structural changes apparent in dementia will therefore have significant consequences for cognitive performance. Despite this, the effects of tauopathy induction in WM has not been explored, nor has the functional consequences of tauopathy been examined in WM. Recent studies highlight the significance of axo-glial signaling in the regulation of axonal myelin (Fields, 2015; Spitzer, Volbracht, Lundgaard, & Karadottir, 2016), a phenomenon that appears to share features with synaptic transmission and is likely to have a comparable sensitivity to pathological forms of tau (Zhou et al., 2017). We here report the effect of tauopathy induction on mature WM structure and function, revealing a novel form of early non-inflammatory ad-axonal myelin disruption associated with transient loss of action potential conduction. During ongoing tauopathy, myelin remodeling subsequently restored excitability and produced a phenotype that is consistent with the microstructural changes apparent in prodromal forms of human dementia.

Materials and Methods

All animal procedures were approved by the Plymouth University

Animal Welfare and Ethical Review Board and conformed to UK home office regulations. rTg4510 tauP301L mice were generated by crossing B6.Cg-Tg(Camk2a-tTA)1Mmay/DboJ mice (stock # 007004) with FVB-Tg(tetO-MAPT*P301L)#Kha/JlwsJ (stock # 015815), both from The Jackson laboratory (USA). B6.Cg-Tg(Camk2a-tTA)1Mmay/DboJ are on a C57Bl/6J background, and were specifically chosen to avoid tet-off DG neurotoxicity (Han et al., 2012). Following genotyping, mice carrying a single copy of both the CamKIIa and MAPT P301L genes were considered rTg4510(+) and mice positive for CamKIIa only were rTg4510(-). Western blot of cell lysates using polyclonal anti human tau (Dako, total tau) reported a 2-fold tau increase in rTG4510(+) relative to rTG4510(-) at 4 months induction. Pregnant animals and offspring ≤P30 (30 post-natal days) were fed doxycycline diet *ad lib*. To induce expression of tauP301L transgene, diet was changed to doxycycline-free at P30 and maintained thereafter (for both rTg4510(+) and the rTg4510(-controls).

Immunostaining.

ONs were transferred to 0.1M phosphate buffered saline (PBS) prior to fixing in 4% paraformaldehyde (PFA: 30 min), cryoprotected (20-30% sucrose for 5 min), transferred to Tissue Tec media (Sigma, UK.) and frozen using ethanol and dry ice. 20µm sections were cut by cryostat, submerged in 0.1M PBS for 5 min and blocked in 0.1M PBS containing 10% goat serum and 0.5% Triton-X for 120 min prior to overnight exposure to primary antibody at 4ºC in the same solution. Monoclonal glial fibrillary acidic protein (GFAP) (Molecular Probes, 1:200), and Ser202 and Thr205 phosphorylated tau (AT8, Thermo Fisher Scientific, UK, 1:1000) were used. Slides were then washed and incubated in the appropriate Alexa conjugated secondary antibody (Molecular Probes, 1:1000). Images were collected using a TCS SP8 confocal microscope (Leica, Germany,60x objective). In all cases, control staining where primary antibody was omitted from the protocol were blank.

Behavioral testing

Novel object recognition was performed as we have described previously (Hall, Yang, Sauchanka, Spillantini, & Anichtchik, 2015) using a Y-maze. After 30 minutes habituation to the testing room, male rTG4510 mice were exposed to two identical objects located in the short arms of Y-maze for 5 minutes and then returned to their home cages. After one hour, mice were individually reintroduced to the Y-maze, where a novel object was introduced alongside the familiar one, and the interaction with the objects (sniffing, touching, biting) was recorded. A discrimination index (D.I.) was calculated as (Tn-Tf)/(Tn+Tf), where Tn was the time spent exploring the novel object and Tf was the time spent exploring the familiar object, both within the 5 minutes. Groups were balanced by randomization of the position of the novel object (left or right side), to avoid side-preferential bias. In addition to the test being performed in a Y maze, recognition memory in these mice was confirmed with additional experiments using the same protocol but within the more commonly

used open square arena, which is more strongly associated with hippocampal function. In this version, the square arena measured 400x 400 x 400mm and had a camera placed overhead, which recorded movement using NORT-3D software (Bioseb, France). Settings in the NORT-3D software were changed so that the maximum distance from the object, for the object exploration to be detected, was 1mm and the maximum angle between head and object was 44^{o}. The maximum exploration duration per trial used was 5 minutes. The NORT-3D software automatically tracked the movement of each mouse and calculated the exploration duration of outlined objects.

Electrophysiology

ON were dissected into artificial cerebrospinal fluid (aCSF) (in mM: NaCl, 126; KCl, 3; NaH_2PO_4, 2; $MgSO_4$, 2; $CaCl_2$, 2; $NaHCO_3$, 26; glucose, 10; pH, 7.45), bubbled with 5% CO_2 / 95% O_2. Compound action potentials (CAPs) were evoked and recorded with glass electrodes and the rectified area, CAP amplitude and conduction latency to first peak used to determine changes in excitability (see(Alix et al., 2012) for further details). CAPs were evoked via square-wave constant current pulses (Iso stim A320, WPI), amplified (Cyber Amp 320, Axon Instruments), subtracted from a parallel differential electrode, filtered (low pass: 800–10000 Hz), digitized (1401 mini, Cambridge Electronic Design) and displayed on a PC running Signal software (Cambridge Electronic Design).

Electron microscopy

Mice were anaesthetized and transcardially perfused for 5 min with cold saline + 5 min 4% PFA in Sorenson's solution. The brain was then removed, hemisected and one hemisphere and the ONs immersion fixed in 2.5% gluteraldehyde/0.1 M Sorensen buffer overnight. Tissue was post-fixed (1% osmium tetroxide) and serially dehydrated prior to epoxy infiltration. Ultrathin sections were counterstained with uranyl acetate and lead citrate prior to examination using a Joel JEM1400 electron microscope. ON were sectioned cross-section (X-S) or long-section (L-S); hippocampi were sectioned in the sagittal plan. A minimum of 4 grid-sections in each of a minimum of 2 specimens were analyzed blind by hand including the tracing of axons, myelin and mitochondria and the measurement of endoplasmic reticulum and myelin layer thickness (Image-J, NIH). G-ratio was calculated by measuring the envelope area around the outermost layer of myelin and the axon, converting these two areas to ideal circles and dividing. Note this will include areas of decompaction within the sheath and the periaxonal space. Myelin thickness, periodicity and periaxonal space width were all measured separately and are presented where relevant. Pre-synaptic vesicle pool envelope size was calculated using a region of interest connecting the outer edges of the pool and the post-synaptic density (PSD), vesicle density was calculated from the number of vesicles within this envelope.

Statistics

Data are mean ± SEM, significance determined by t-test or ANOVA with Holm-Šídák *post hoc*-test as appropriate. All data were collected blind and significance tested vs., littermates. * P = 0.05, ** P = 0.01, *** P = 0.001.

Results

Hyper-phosphorylated tau was evident from 2 months of age (1 month transgene induction) in rTG4510(+) littermates in the dentate gyrus (DG) (Fig 1 A-D). As in prior studies using the model (Ramsden et al., 2005; Santacruz et al., 2005), granule cell loss in this structure was evident at 9 months of induction (Fig 1 G, H). No astrocyte reaction was apparent during the first 3 months of induction assessed via immuno-staining for GFAP (Fig 1 E, F) or via ultrastructural assessment of reactive changes in astrocytes identified using well established structural criteria (Fig S 1). DG granule neurons receive synaptic input from the entorhinal cortex via perforant path (PP) axons which terminate in the DG molecular layer (ML). The corresponding presynaptic vesicular pool envelope area, pool vesicle density and post-synaptic density length were not significantly altered at 1 or 3 months induction (Fig 1 I, J). Despite the absence of astrogliosis or changes in synaptic morphology, the myelinated axons of the PP that project these presynaptic elements within the DG ML exhibited significant myelin thinning at 1 month of transgene induction (Fig 1 K, L). G-ratio increased from 0.772 +/- 0.057 to 0.8001 +/-0.060 ($P<0.05$) but no other form of myelin pathology was apparent.

Figure 1

Tauopathy induction can interfere with synaptic transmission via the direct action of tau upon vesicle motility and release (Zhou et al., 2017), while axonal vesicular release may mediate axo-myelinic signaling (e.g., (Kukley, Capetillo-Zarate, & Dietrich, 2007), representing a potential mechanisms leading to early myelin changes such as the thinning apparent in Figure 1 in the rTG43510(+) mice. Myelinated DG ML PP axons in tau(-) littermates contained both clustered and dispersed axoplasmic vesicles of similar size to those present in their pre-synaptic endings (20-40 nm), and total axoplasmic vesicle density was reduced in these axons at 1 and 3 months of mutant tau induction (Fig 2 A-C). Myelin thinning, such as that observed at 1 month of mutant tau induction, is a feature of remyelination. Remyelination following focal demyelination can be complete within 6 weeks (Woodruff & Franklin, 1999), suggesting that a cycle of myelin pathology and recovery may largely precede the end of the 1 month induction period in the rTG4510 mutant. Indeed, myelin damage was widespread in ammonic path (AP) axons in the para-ventricular alveus adjacent to the CA2 region of the hippocampus (Fig 2 D, E), which take a significantly longer route from the entorhinal cortex than axons of the PP (Deller, Adelmann, Nitsch, & Frotscher, 1996), and may therefore exhibit relatively delayed myelin pathology. Structural changes in these axons included ad-axonal myelin disruption while axonal mitochondria retained a normal morphology and there was no sign of a glial reaction. The myelin pathology found in the alveus at 1 month induction was highly region specific with no myelinated axon pathology evident in adjacent white or gray matter structures. Neuronal and glial populations in the CA2 stratum oriens showed no structural deficits or myelin changes (Fig 2 F), but thick neuronal

projections within the neuropil contained large numbers of mitochondria exhibiting the mitochondria-on-a-stick (MOAS) morphology, an early sign of neuronal stress (L. Zhang et al., 2016) which was rare in the same region of mutant tau (-) littermates (Fig 2 F, G red arrows).

Figure 2

The early features of the functional and structural pathology in WM were examined in greater detail in the isolated optic nerve (ON), where myelinated axons run in parallel in a neuronal synapse-free WM structure and hyperphosphorylated tau was present in axons and absent in astrocytes following mutant tau induction (Fig 3 A). ON excitability was compromised after 1-2 months of mutant tau induction, showing a 70-80% loss of CAP area and amplitude and a significant increase in conduction latency (Fig 3 B, C). Excitability recovered over 6-10 months of mutant tau induction although a significant loss of CAP area was still evident at 10 months (Fig 3 B, C). This transient functional failure was not accompanied by frank ON de-myelination assessed via fluoromyelin staining, but the mean myelin sheath width was expanded at 1 month of induction producing an increase in myelin staining of whole sections (Fig 3 D). The rapid onset and subsequent resolution of the structural and functional compromise of DG and ON WM was paralleled by a decline in performance of a novel object recognition test (Fig 3 F). This neurological deficit may reflect compromised ON function or a combination of this and a decline in synaptic processing. Since the CamkII promoter is active in in olfactory and auditory sensory neurons in addition to retinal ganglion cells (Wang, Zhang, Szabo, & Sun, 2013); (Zou, Greer, & Firestein, 2002), dissecting sensory and cognitive effects of WM functional loss is not possible in the rTG4510 inducible tauopathy model. However, since early sensory decline is a common feature of dementia, reduced performance of a visual-cognitive test whether from sensory or cognitive failure has clear clinical relevance.

Figure 3

ON axon G-ratio was significantly lower after 1 month of transgene induction compared to littermate controls. This was the case whether G-ratio was calculated from the idealized axon and myelin diameters derived from their area or their perimeter (Fig 4 A-C). A low G-ratio indicates a relative expansion of the myelin sheath and is often a result of myelin decompaction/splitting. However, myelin thickness, periodicity and the number of layers in regions of compact myelin were not affected at any axon diameter in rTG4510(+) littermates (Fig 4 D-G). In addition, there was no change in the width of the peri-axonal space between the inner myelin layer and the internodal axolemma, a parameter that can also effect the G-ratio calculation (Fig 4 E-G). Since G-ratio is related to axon diameter, we determined the axon diameter spectrum in tau (+) and (-) littermates and found no significant differences (Fig 4 H). The G-ratio increase was solely accounted for by the presence of focal structural defects in the ad-axonal myelinic and axoplasmic peri-axonal membranes, apparent in low (Fig 4 A) and high power (Fig 5) ultramicrographs. The features of these focal defects

included a degree of axoplasmic infolding associated with an expansion of oligodendrocyte inner tongue process with preservation of the peri-axonal space and splitting/blebbing of the ad-axonal myelin. Damaged myelin was often located within the expanded inner tongue process as where lamina bodies that occasionally enclosed large vacuoles apparent in L-S (Fig 5 A-D). In X-S, the lamina bodies often had features described in other forms of WM injury as dystrophic axons (Fig 5 E), but the intra-axonal nature of these structures observed in L-S excluded this possibility.

Axoplasmic mitochondria had a normal structure (Fig 5 A), but were significantly depleted in tau(+) axons and had a significant increase in area (Fig 5 F, G). This effect was not found in the mitochondria of accompanying glial cells (Fig 5 G). Mitochondrial compromise may be a common factor in many forms of axonal pathology (Coleman, 2005), but the preservation of cytoskeletal elements such as microtubules are inconsistent with significant axonal damage associated with this change in mitochondrial size (Fig 5). Axons with an electron-dense axoplasm were present following 1 month of transgene induction, and frequently exhibited myelin structural abnormalities similar to those in axons with a normal axoplasmic density (Fig S 2).

Figure 4, 5

As in DG ML PP myelinated axons, sub-myelinic clusters of 20-40 nm axon vesicles are apparent in tau(-) rTG4510 ON axons (Fig 6 A). Vesicle clusters often incorporated short cylindrical profiles and some less spherical structures of a similar diameter. Similar clusters were apparent in X-S, but are hard to distinguish from microtubules which have a similar diameter. Axoplasmic vesicle clusters (>5 vesicles) were less focal and contained fewer elements in tau(+) littermates at 1 month induction (Fig 6 B), confirmed in a nearest-neighbor analysis of vesicle distribution within clusters and in the mean cluster size (Fig 6 C, D). Individual and small groups of axoplasmic vesicles were also observed in both groups. ON nodes of Ranvier in tau(-) littermates exhibited a normal morphology with compact myelin reducing in a series of end-loops and a relatively unobstructed nodal axoplasm with a mean diameter of 0.79 (+/- 0.11 μm; Fig 6 E, right). In tau(+) ON, nodal axoplasm was often cluttered with inclusions and although absolute node diameter was not significantly different to that in tau(-) littermates (0.792 +/- 0.11 μ m; Fig 6 E, left), the ratio of peri-nodal/nodal axon diameter was significantly higher in tau(+) ON indicating swelling or expansion of the nodal axolemma into the peri-nodal space (Fig 6 F).

Figure 6

Functional recovery from the acute pathology associated with mutant tau induction was paralleled by resolution of the focal myelin damage in the ON. Axon G-ratio across the diameter spectrum gradually shifted from the low values associated with myelin pathology at one month induction to high values at 10 months induction, typical of the thin myelin sheaths of remyelinated axons (Peters, 2009; Prineas & Connell, 1979) (Fig 7 A, B). The proportion of node of Ranvier profiles relative to internodal myelin profiles was

significantly elevated at 1, 3 and 10 months of transgene induction (Fig 7 C), demonstrating a proliferation of short inter-nodes that is also typical of remyelinated axons. Despite this remyelinated axon phenotype, there was no significant change in axon density at any period of transgene induction (Fig 6 D), and demyelinated axon cylinders were absent at all time points. Acute mutant tau induction therefore evokes rapid and severe myelin injury followed by myelin remodeling and repair with the features of remyelination but without myelin loss. After 10 months of transgene induction limited focal dark expansions of myelin where apparent (Fig 7 F), and low-power images reveal no wide-scale pathology other than myelin thinning (Fig 7 G). There were no signs of inflammatory changes in the ON at any time point and glia soma and processes exhibited no overt changes following mutant tau induction at any time point (Fig 8).

Figure 7, 8

Discussion

Constitutive expression of mutant tau is associated with a variety of pathological WM phenotypes including focal axon swelling and necrosis (Brunden et al., 2010; Gasparini et al., 2011; Leroy et al., 2007; Probst et al., 2000; Sahara et al., 2014; Spittaels et al., 1999), oligodendrocyte injury (Lin et al., 2005; Ludvigson, Luebke, Lewis, & Peters, 2011; Zehr et al., 2004) and myelin disruption (Maurin et al., 2014; Sahara et al., 2014); anisotropic changes typical of general myelin disruption are apparent at 2.5 months in the constitutively active rTg4510 mouse (Sahara et al., 2014). Focal axonal swelling, axon necrosis, generalized myelin disruption, glial soma pathology and reactive glial and inflammatory changes were not observed at any age in either the hippocampus or ON following tauopathy induced at one month, a major difference that reflects the significance of maturation on pathogenesis as found in many forms of CNS pathology (e.g., (R. Fern, Davis, Waxman, & Ransom, 1998)). It is not known if constitutive tauopathy evokes loss of WM function, but cognitive decline in these models post-dates some of the most significant WM structural changes described in earlier studies and functionally significant WM failure is therefore unlikely.

In the current analysis, tauopathy induction evoked significant action potential conduction loss apparent after 1 month in the ON that was largely resolved after 10 months of continued induction. This was accompanied by disorganization in the morphological arrangement of the axo-myelinic interface and a decline in performance of a functional memory test with no structural change in ML DG synapses. Myelinated axons within the hippocampus exhibited similar structural changes evolving over a more rapid time-course. Saltatory action potential conduction is exquisitely sensitive to disruption of the myelin sheath, with even quite subtle myelin changes associated with significant loss of excitability (e.g., (Bagchi et al., 2014)). The acute ad-axonal myelin pathology evoked following mutant tau induction was clearly sufficient to compromise saltatory conduction in the affected axons, and since synaptic structures were not affected this presumably is responsible for the initial decline in novel recognition test performance. In both the hippocampus and optic nerve, a recovery phase progressed during continued tauopathy induction involved myelin remodeling and resulted in a thinner

myelin sheath and, in the optic nerve, shorter nodal distance, a phenotype typical of axons in the re-myelinated and the aged CNS (Peters, 2009; Prineas & Connell, 1979). This recovery phase partially restored novel recognition test performance, although a trend to a deficit remained and was significant after 10 months of induction. Myelin changes of this type can restore action potential conduction to within normal limits following demyelination (Wu, Williams, Delaney, Sherman, & Brophy, 2012), but impose an energetic cost that is likely to leave WM vulnerable to further functional decline (Smith, 2006; Zambonin et al., 2011).

The *MAPT* mutation present in the rTG4510 model disrupts axoplasmic transport (Majid et al., 2014; Santacruz et al., 2005). In normal WM, axoplasmic transport traffics organelles, gene products, proteins, synaptic vesicle components and trophic support factors from the soma to the synapse and interruption of this flow may have consequences for the functional viability of axons (Noble, Hanger, Miller, & Lovestone, 2013). For example, failure to appropriately deliver and target mitochondria may compromise axonal energy production, leading to "virtual anoxia" as hypothesized in multiple sclerosis (Trapp & Stys, 2009). A significant reduction in the number of mitochondria in the axoplasm following mutant tau induction was found in the current study, but this was compensated by an axon-specific increase in mitochondrial size. Acute tauopathy therefore appears to evoke mitochondrial fusion, a protective response to cellular stress described in many cell types (Youle & van der Bliek, 2012), rather than producing a loss or disruption of mitochondria leading to failure of energy supply. The preservation of microtubules, axolemma, and the para-nodal morphological arrangement are also inconsistent with the disruption of ionic homeostasis that characterize axon injury produced by energy compromise (R. F. Fern, Matute, & Stys, 2014).

In addition to potential effects upon mitochondria, arrest of axoplasmic transport following tau induction will interrupt the delivery of vesicular components to the axon itself and this may be the cause of the observed disruption in axoplasmic vesicle distribution. Independently of effects upon transport, pathogenic tau will bind directly to vesicles to disrupt mobility and fusion (Zhou et al., 2017). Tauopathy induction is therefore likely to compromise axo-glial signaling mediated via vesicular release, a phenomenon implicated in myelin plasticity (Fields, 2015; Spitzer et al., 2016). Myelin exhibits a significant degree of plasticity in the mature CNS (Fields, 2015; Young et al., 2013; Zatorre, Fields, & Johansen-Berg, 2012). For example, myelination increases following learning (Sampaio-Baptista et al., 2013; Scholz, Klein, Behrens, & Johansen-Berg, 2009), and is reduced in a number of psychological conditions and following social isolation (Lener & Iosifescu, 2015; Liu et al., 2012; Seitz et al., 2016). Axon stimulation is linked to an expansion in myelin sheath thickness (Gibson et al., 2014), while axonal action potentials evoke vesicular glutamate release to promote myelination via oligodendrocyte glutamate receptors (Wake, Lee, & Fields, 2011). Block of vesicular glutamate release replicates the internodal shortening effect of visual deprivation in the ON (Etxeberria et al., 2016). The myelin thinning and internodal shortening that followed tauopathy induction is therefore consistent with the predicted effect of axo-glial vesicular signal interruption. Recent findings have shown that oligodendrocyte processes continually intercalate

internodal segments into established myelin sheaths (Young et al., 2013), and that the newly deposited myelin generated in this fashion forms short internodes with thin myelin (Chang, Redmond, & Chan, 2016). Despite ongoing and extensive myelin re-modeling, sections of demyelinated axons were not found following tauopathy induction in the current work, indicating that process intercalation of this type contributes to nodal shortening in the functionally restored axons. The initial ad-axonal myelin damage observed in ON and AP axons may represent an early phase of myelin remodeling, with myelin removal leading to a thinner myelin sheath. Interruption in axo-glial glutamate signaling is also likely to negatively affect myelin energy utilization, with damaging consequences at latter age points (Saab et al., 2016).

Failure of WM function during early tauopathy will disrupt neural circuits and compromise neurological function. The current findings suggest this phenomenon is likely to make a significant contribution to the earliest clinical deficit in dementia. The transient nature of the effects described in the results may mitigate their clinical consequences, but the findings show that longer WM pathways suffer more extended pathology (ON>AP>PP), and large human WM structures are correspondingly long. Furthermore, tauopathy induction produces relatively synchronized mutant tau expression within a particular tract and therefore the recovery phase described in the results is also synchronized. In contrast, clinical dementia is an ongoing disorder, where WM failure may contribute to symptomology throughout the lifetime of the patient. The post-tauopathy phenotype here described here is novel outside the fields of aging and multiple sclerosis and the associated elevation in energy demand that it imposes may also contribute to disease progression. The structural analysis revealed a correlation between axonal vesicle organization and ad-axonal myelin pathology. While potentially causal, these effects may stem from a common pathogenic trigger. For example, recent evidence shows that early mutant tau induction leads to occlusion of synaptic transmission via the direct actions of tau upon vesicle release (Zhou et al., 2017). Potentially, such early synaptic occlusion may uncouple WM connections and evoke the structural and functional decline described in the results. However, the most direct conclusion from the current findings is that early transient WM injury is responsible for a transient neurological deficit, placing the phenomena at the leading edge of dementia progression with potential consequences for the subsequent health of gray matter synapses.

References

Alix, J. J., Zammit, C., Riddle, A., Meshul, C. K., Back, S. A., Valentino, M., & Fern, R. (2012). Central axons preparing to myelinate are highly sensitive [corrected] to ischemic injury. *Ann Neurol, 72*(6), 936-951. doi:10.1002/ana.23690

Amlien, I. K., & Fjell, A. M. (2014). Diffusion tensor imaging of white matter degeneration in Alzheimer's disease and mild cognitive impairment. *Neuroscience, 276*, 206-215. doi:10.1016/j.neuroscience.2014.02.017

Back, S. A., Kroenke, C. D., Sherman, L. S., Lawrence, G., Gong, X., Taber, E. N., . . . Montine, T. J. (2011). White matter lesions defined by diffusion tensor imaging in older adults. *Ann Neurol, 70*(3), 465-476. doi:10.1002/ana.22484

Bagchi, B., Al-Sabi, A., Kaza, S., Scholz, D., O'Leary, V. B., Dolly, J. O., & Ovsepian, S. V. (2014). Disruption of myelin leads to ectopic expression of K(V)1.1 channels with abnormal conductivity of optic nerve axons in a cuprizone-induced model of demyelination. *PLoS One, 9*(2), e87736. doi:10.1371/journal.pone.0087736

Bendlin, B. B., Ries, M. L., Canu, E., Sodhi, A., Lazar, M., Alexander, A. L., . . . Johnson, S. C. (2010). White matter is altered with parental family history of Alzheimer's disease. *Alzheimers Dement, 6*(5), 394-403. doi:10.1016/j.jalz.2009.11.003

Binder, L. I., Frankfurter, A., & Rebhun, L. I. (1985). The Distribution of Tau in the Mammalian Central Nervous-System. *Journal of Cell Biology, 101*(4), 1371-1378. doi:DOI 10.1083/jcb.101.4.1371

Boeve, B. F., & Hutton, M. (2008). Refining frontotemporal dementia with parkinsonism linked to chromosome 17: introducing FTDP-17 (MAPT) and FTDP-17 (PGRN). *Arch Neurol, 65*(4), 460-464. doi:10.1001/archneur.65.4.460

Brier, M. R., Thomas, J. B., Snyder, A. Z., Benzinger, T. L., Zhang, D., Raichle, M. E., . . . Ances, B. M. (2012). Loss of intranetwork and internetwork resting state functional connections with Alzheimer's disease progression. *J Neurosci, 32*(26), 8890-8899. doi:10.1523/JNEUROSCI.5698-11.2012

Brun, A., & Englund, E. (1986). A white matter disorder in dementia of the Alzheimer type: a pathoanatomical study. *Ann Neurol, 19*(3), 253-262. doi:10.1002/ana.410190306

Brunden, K. R., Zhang, B., Carroll, J., Yao, Y., Potuzak, J. S., Hogan, A. M., . . . Trojanowski, J. Q. (2010). Epothilone D improves microtubule density, axonal integrity, and cognition in a transgenic mouse model of tauopathy. *J Neurosci, 30*(41), 13861-13866. doi:10.1523/JNEUROSCI.3059-10.2010

Chang, K. J., Redmond, S. A., & Chan, J. R. (2016). Remodeling myelination: implications for mechanisms of neural plasticity. *Nat Neurosci, 19*(2), 190-197. doi:10.1038/nn.4200

Coleman, M. (2005). Axon degeneration mechanisms: commonality amid diversity. *Nat Rev Neurosci, 6*(11), 889-898. doi:10.1038/nrn1788

de la Monte, S. M. (1989). Quantitation of cerebral atrophy in preclinical and end-stage Alzheimer's disease. *Ann Neurol, 25*(5), 450-459. doi:10.1002/ana.410250506

Deller, T., Adelmann, G., Nitsch, R., & Frotscher, M. (1996). The alvear pathway of the rat hippocampus. *Cell Tissue Res, 286*(3), 293-303. doi:DOI 10.1007/s004410050699

Etxeberria, A., Hokanson, K. C., Dao, D. Q., Mayoral, S. R., Mei, F., Redmond, S. A., . . . Chan, J. R. (2016). Dynamic Modulation of Myelination in Response to Visual Stimuli Alters Optic Nerve Conduction Velocity. *J Neurosci, 36*(26), 6937-6948. doi:10.1523/JNEUROSCI.0908-16.2016

Fern, R., Davis, P., Waxman, S. G., & Ransom, B. R. (1998). Axon conduction and survival in CNS white matter during energy deprivation: a developmental study. *J Neurophysiol, 79*(1), 95-105.

Fern, R. F., Matute, C., & Stys, P. K. (2014). White matter injury: Ischemic and nonischemic. *Glia, 62*(11), 1780-1789. doi:10.1002/glia.22722

Fields, R. D. (2015). A new mechanism of nervous system plasticity: activity-dependent myelination. *Nat Rev Neurosci, 16*(12), 756-767. doi:10.1038/nrn4023

Gasparini, L., Crowther, R. A., Martin, K. R., Berg, N., Coleman, M., Goedert, M., & Spillantini, M. G. (2011). Tau inclusions in retinal ganglion cells of human P301S tau transgenic mice: effects on axonal viability. *Neurobiol Aging, 32*(3), 419-433. doi:10.1016/j.neurobiolaging.2009.03.002

Gibson, E. M., Purger, D., Mount, C. W., Goldstein, A. K., Lin, G. L., Wood, L. S., . . . Monje, M. (2014). Neuronal activity promotes oligodendrogenesis and adaptive myelination in the mammalian brain. *Science, 344*(6183), 1252304. doi:10.1126/science.1252304

Goedert, M., & Spillantini, M. G. (2006). A century of Alzheimer's disease. *Science, 314*(5800), 777-781. doi:10.1126/science.1132814

Gold, B. T., Johnson, N. F., Powell, D. K., & Smith, C. D. (2012). White matter integrity and vulnerability to Alzheimer's disease: preliminary findings and future directions. *Biochim Biophys Acta, 1822*(3), 416-422. doi:10.1016/j.bbadis.2011.07.009

Hall, K., Yang, S., Sauchanka, O., Spillantini, M. G., & Anichtchik, O. (2015). Behavioural deficits in transgenic mice expressing human truncated (1-120 amino acid) alpha-synuclein. *Exp Neurol, 264*, 8-13. doi:10.1016/j.expneurol.2014.11.003

Han, H. J., Allen, C. C., Buchovecky, C. M., Yetman, M. J., Born, H. A., Marin, M. A., . . . Jankowsky, J. L. (2012). Strain background influences neurotoxicity and behavioral abnormalities in mice expressing the tetracycline transactivator. *J Neurosci, 32*(31), 10574-10586. doi:10.1523/JNEUROSCI.0893-12.2012

Harada, A., Oguchi, K., Okabe, S., Kuno, J., Terada, S., Ohshima, T., . . . Hirokawa, N. (1994). Altered microtubule organization in small-calibre axons of mice lacking tau protein. *Nature, 369*(6480), 488-491. doi:10.1038/369488a0

Kukley, M., Capetillo-Zarate, E., & Dietrich, D. (2007). Vesicular glutamate release from axons in white matter. *Nat Neurosci, 10*(3), 311-320. doi:10.1038/nn1850

Lener, M. S., & Iosifescu, D. V. (2015). In pursuit of neuroimaging biomarkers to guide treatment selection in major depressive disorder: a review of the literature. *Ann N Y Acad Sci, 1344*, 50-65. doi:10.1111/nyas.12759

Leroy, K., Bretteville, A., Schindowski, K., Gilissen, E., Authelet, M., De Decker, R., . . . Brion, J. P. (2007). Early axonopathy preceding neurofibrillary tangles

in mutant tau transgenic mice. *Am J Pathol, 171*(3), 976-992. doi:10.2353/ajpath.2007.070345
Lin, W. L., Zehr, C., Lewis, J., Hutton, M., Yen, S. H., & Dickson, D. W. (2005). Progressive white matter pathology in the spinal cord of transgenic mice expressing mutant (P301L) human tau. *J Neurocytol, 34*(6), 397-410. doi:10.1007/s11068-006-8726-0
Liu, J., Dietz, K., DeLoyht, J. M., Pedre, X., Kelkar, D., Kaur, J., . . . Casaccia, P. (2012). Impaired adult myelination in the prefrontal cortex of socially isolated mice. *Nat Neurosci, 15*(12), 1621-1623. doi:10.1038/nn.3263
Ludvigson, A. E., Luebke, J. I., Lewis, J., & Peters, A. (2011). Structural abnormalities in the cortex of the rTg4510 mouse model of tauopathy: a light and electron microscopy study. *Brain Struct Funct, 216*(1), 31-42. doi:10.1007/s00429-010-0295-4
Majid, T., Ali, Y. O., Venkitaramani, D. V., Jang, M. K., Lu, H. C., & Pautler, R. G. (2014). In vivo axonal transport deficits in a mouse model of fronto-temporal dementia. *Neuroimage Clin, 4*, 711-717. doi:10.1016/j.nicl.2014.02.005
Maurin, H., Chong, S. A., Kraev, I., Davies, H., Kremer, A., Seymour, C. M., . . . Van Leuven, F. (2014). Early structural and functional defects in synapses and myelinated axons in stratum lacunosum moleculare in two preclinical models for tauopathy. *PLoS One, 9*(2), e87605. doi:10.1371/journal.pone.0087605
Noble, W., Hanger, D. P., Miller, C. C., & Lovestone, S. (2013). The importance of tau phosphorylation for neurodegenerative diseases. *Front Neurol, 4*, 83. doi:10.3389/fneur.2013.00083
Peters, A. (2009). The effects of normal aging on myelinated nerve fibers in monkey central nervous system. *Front Neuroanat, 3*, 11. doi:10.3389/neuro.05.011.2009
Prineas, J. W., & Connell, F. (1979). Remyelination in multiple sclerosis. *Ann Neurol, 5*(1), 22-31. doi:10.1002/ana.410050105
Probst, A., Gotz, J., Wiederhold, K. H., Tolnay, M., Mistl, C., Jaton, A. L., . . . Goedert, M. (2000). Axonopathy and amyotrophy in mice transgenic for human four-repeat tau protein. *Acta Neuropathol, 99*(5), 469-481.
Provenzano, F. A., Muraskin, J., Tosto, G., Narkhede, A., Wasserman, B. T., Griffith, E. Y., . . . Alzheimer's Disease Neuroimaging, I. (2013). White matter hyperintensities and cerebral amyloidosis: necessary and sufficient for clinical expression of Alzheimer disease? *JAMA Neurol, 70*(4), 455-461. doi:10.1001/jamaneurol.2013.1321
Ramsden, M., Kotilinek, L., Forster, C., Paulson, J., McGowan, E., SantaCruz, K., . . . Ashe, K. H. (2005). Age-dependent neurofibrillary tangle formation, neuron loss, and memory impairment in a mouse model of human tauopathy (P301L). *Journal of Neuroscience, 25*(46), 10637-10647. doi:10.1523/Jneurosci.3279-05.2005
Roher, A. E., Weiss, N., Kokjohn, T. A., Kuo, Y. M., Kalback, W., Anthony, J., . . . Beach, T. (2002). Increased A beta peptides and reduced cholesterol and myelin proteins characterize white matter degeneration in Alzheimer's disease. *Biochemistry, 41*(37), 11080-11090.
Saab, A. S., Tzvetavona, I. D., Trevisiol, A., Baltan, S., Dibaj, P., Kusch, K., . . . Nave, K. A. (2016). Oligodendroglial NMDA Receptors Regulate Glucose Import

and Axonal Energy Metabolism. *Neuron, 91*(1), 119-132. doi:10.1016/j.neuron.2016.05.016
Sahara, N., Perez, P. D., Lin, W. L., Dickson, D. W., Ren, Y., Zeng, H., . . . Febo, M. (2014). Age-related decline in white matter integrity in a mouse model of tauopathy: an in vivo diffusion tensor magnetic resonance imaging study. *Neurobiol Aging, 35*(6), 1364-1374. doi:10.1016/j.neurobiolaging.2013.12.009
Sampaio-Baptista, C., Khrapitchev, A. A., Foxley, S., Schlagheck, T., Scholz, J., Jbabdi, S., . . . Johansen-Berg, H. (2013). Motor skill learning induces changes in white matter microstructure and myelination. *J Neurosci, 33*(50), 19499-19503. doi:10.1523/JNEUROSCI.3048-13.2013
Santacruz, K., Lewis, J., Spires, T., Paulson, J., Kotilinek, L., Ingelsson, M., . . . Ashe, K. H. (2005). Tau suppression in a neurodegenerative mouse model improves memory function. *Science, 309*(5733), 476-481. doi:10.1126/science.1113694
Schmahmann, J. D., Smith, E. E., Eichler, F. S., & Filley, C. M. (2008). Cerebral white matter: neuroanatomy, clinical neurology, and neurobehavioral correlates. *Ann N Y Acad Sci, 1142*, 266-309. doi:10.1196/annals.1444.017
Scholz, J., Klein, M. C., Behrens, T. E., & Johansen-Berg, H. (2009). Training induces changes in white-matter architecture. *Nat Neurosci, 12*(11), 1370-1371. doi:10.1038/nn.2412
Seitz, J., Zuo, J. X., Lyall, A. E., Makris, N., Kikinis, Z., Bouix, S., . . . Kubicki, M. (2016). Tractography Analysis of 5 White Matter Bundles and Their Clinical and Cognitive Correlates in Early-Course Schizophrenia. *Schizophr Bull, 42*(3), 762-771. doi:10.1093/schbul/sbv171
Skillback, T., Zetterberg, H., Blennow, K., & Mattsson, N. (2013). Cerebrospinal fluid biomarkers for Alzheimer disease and subcortical axonal damage in 5,542 clinical samples. *Alzheimers Res Ther, 5*(5), 47. doi:10.1186/alzrt212
Smith, K. J. (2006). Axonal protection in multiple sclerosis--a particular need during remyelination? *Brain, 129*(Pt 12), 3147-3149. doi:10.1093/brain/awl323
Spittaels, K., Van den Haute, C., Van Dorpe, J., Bruynseels, K., Vandezande, K., Laenen, I., . . . Van Leuven, F. (1999). Prominent axonopathy in the brain and spinal cord of transgenic mice overexpressing four-repeat human tau protein. *Am J Pathol, 155*(6), 2153-2165. doi:10.1016/S0002-9440(10)65533-2
Spitzer, S., Volbracht, K., Lundgaard, I., & Karadottir, R. T. (2016). Glutamate signalling: A multifaceted modulator of oligodendrocyte lineage cells in health and disease. *Neuropharmacology*. doi:10.1016/j.neuropharm.2016.06.014
Teipel, S., Grothe, M. J., Zhou, J., Sepulcre, J., Dyrba, M., Sorg, C., & Babiloni, C. (2016). Measuring Cortical Connectivity in Alzheimer's Disease as a Brain Neural Network Pathology: Toward Clinical Applications. *J Int Neuropsychol Soc, 22*(2), 138-163. doi:10.1017/S1355617715000995
Trapp, B. D., & Stys, P. K. (2009). Virtual hypoxia and chronic necrosis of demyelinated axons in multiple sclerosis. *Lancet Neurol, 8*(3), 280-291. doi:10.1016/S1474-4422(09)70043-2

Wake, H., Lee, P. R., & Fields, R. D. (2011). Control of local protein synthesis and initial events in myelination by action potentials. *Science, 333*(6049), 1647-1651. doi:10.1126/science.1206998

Wang, X., Zhang, C., Szabo, G., & Sun, Q. Q. (2013). Distribution of CaMKIIalpha expression in the brain in vivo, studied by CaMKIIalpha-GFP mice. *Brain Res, 1518*, 9-25. doi:10.1016/j.brainres.2013.04.042

Woodruff, R. H., & Franklin, R. J. (1999). Demyelination and remyelination of the caudal cerebellar peduncle of adult rats following stereotaxic injections of lysolecithin, ethidium bromide, and complement/anti-galactocerebroside: a comparative study. *Glia, 25*(3), 216-228.

Wu, L. M., Williams, A., Delaney, A., Sherman, D. L., & Brophy, P. J. (2012). Increasing internodal distance in myelinated nerves accelerates nerve conduction to a flat maximum. *Curr Biol, 22*(20), 1957-1961. doi:10.1016/j.cub.2012.08.025

Yin, R. H., Tan, L., Liu, Y., Wang, W. Y., Wang, H. F., Jiang, T., . . . Yu, J. T. (2015). Multimodal Voxel-Based Meta-Analysis of White Matter Abnormalities in Alzheimer's Disease. *J Alzheimers Dis, 47*(2), 495-507. doi:10.3233/JAD-150139

Youle, R. J., & van der Bliek, A. M. (2012). Mitochondrial fission, fusion, and stress. *Science, 337*(6098), 1062-1065. doi:10.1126/science.1219855

Young, K. M., Psachoulia, K., Tripathi, R. B., Dunn, S. J., Cossell, L., Attwell, D., . . . Richardson, W. D. (2013). Oligodendrocyte dynamics in the healthy adult CNS: evidence for myelin remodeling. *Neuron, 77*(5), 873-885. doi:10.1016/j.neuron.2013.01.006

Zambonin, J. L., Zhao, C., Ohno, N., Campbell, G. R., Engeham, S., Ziabreva, I., . . . Mahad, D. J. (2011). Increased mitochondrial content in remyelinated axons: implications for multiple sclerosis. *Brain, 134*(Pt 7), 1901-1913. doi:10.1093/brain/awr110

Zatorre, R. J., Fields, R. D., & Johansen-Berg, H. (2012). Plasticity in gray and white: neuroimaging changes in brain structure during learning. *Nat Neurosci, 15*(4), 528-536. doi:10.1038/nn.3045

Zehr, C., Lewis, J., McGowan, E., Crook, J., Lin, W. L., Godwin, K., . . . Hutton, M. (2004). Apoptosis in oligodendrocytes is associated with axonal degeneration in P301L tau mice. *Neurobiol Dis, 15*(3), 553-562. doi:10.1016/j.nbd.2003.12.011

Zempel, H., & Mandelkow, E. (2014). Lost after translation: missorting of Tau protein and consequences for Alzheimer disease. *Trends Neurosci, 37*(12), 721-732. doi:10.1016/j.tins.2014.08.004

Zetterberg, H., Skillback, T., Mattsson, N., Trojanowski, J. Q., Portelius, E., Shaw, L. M., . . . Alzheimer's Disease Neuroimaging, I. (2015). Association of Cerebrospinal Fluid Neurofilament Light Concentration With Alzheimer Disease Progression. *JAMA Neurol*, 1-8. doi:10.1001/jamaneurol.2015.3037

Zhang, B., Xu, Y., Zhu, B., & Kantarci, K. (2014). The role of diffusion tensor imaging in detecting microstructural changes in prodromal Alzheimer's disease. *CNS Neurosci Ther, 20*(1), 3-9. doi:10.1111/cns.12166

Zhang, L., Trushin, S., Christensen, T. A., Bachmeier, B. V., Gateno, B., Schroeder, A., . . . Trushina, E. (2016). Altered brain energetics induces mitochondrial fission arrest in Alzheimer's Disease. *Sci Rep, 6*. doi:ARTN 18725

10.1038/srep18725
Zhou, L., McInnes, J., Wierda, K., Holt, M., Herrmann, A. G., Jackson, R. J., . . . Verstreken, P. (2017). Tau association with synaptic vesicles causes presynaptic dysfunction. *Nat Commun, 8*, 15295. doi:10.1038/ncomms15295
https://www.nature.com/articles/ncomms15295 - supplementary-information
Zou, D. J., Greer, C. A., & Firestein, S. (2002). Expression pattern of alpha CaMKII in the mouse main olfactory bulb. *J Comp Neurol, 443*(3), 226-236.

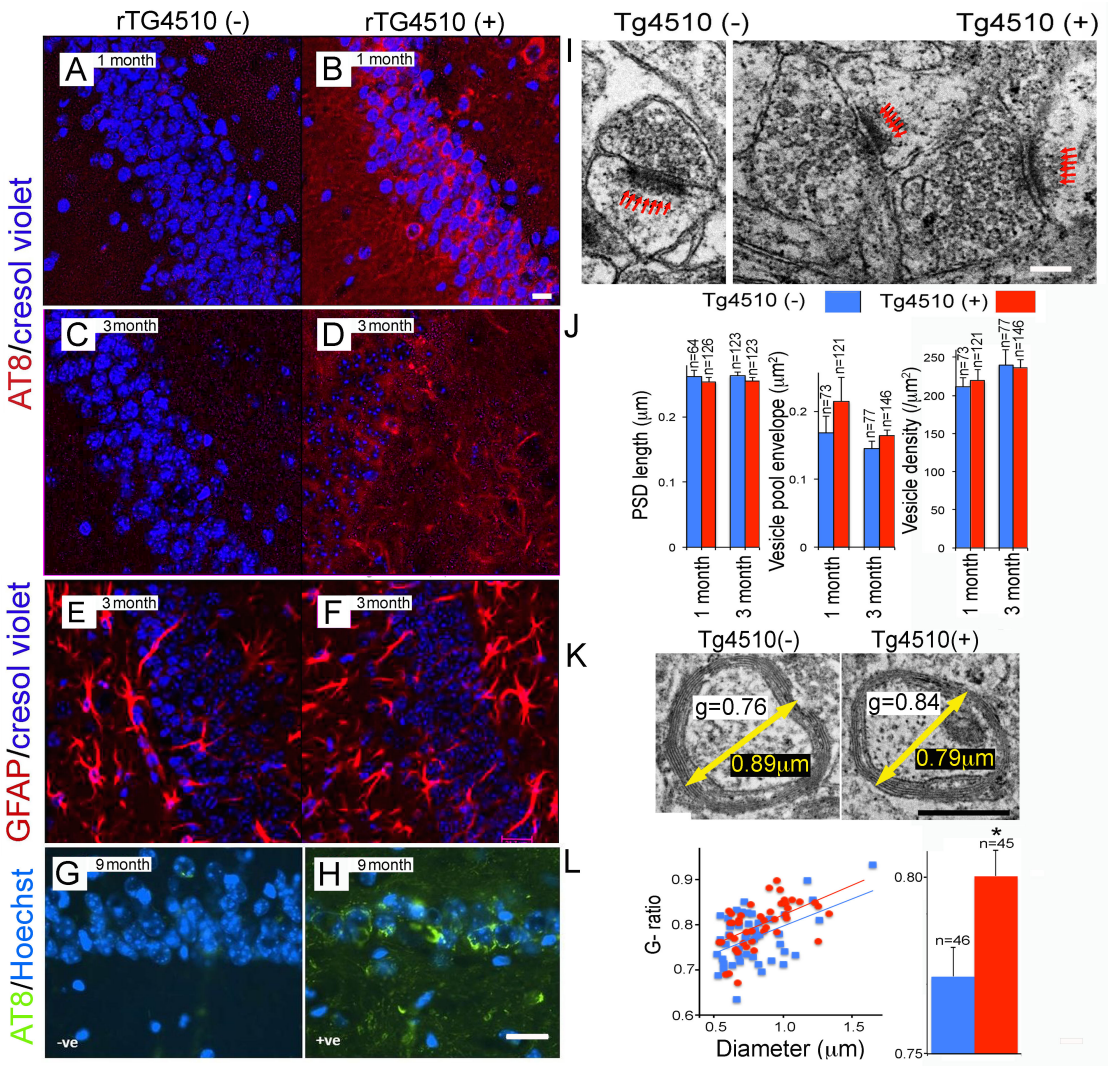

Figure 1. Early structural changes in the hippocampus following mutant tau induction. A-D: Tau hyper-phosphorylation detected with AT8 reactivity in DG granule neurons after 1 month (A, B) and 3 months (C, D) of induction. E, F: No significant astrocyte reaction apparent with GFAP staining of the same region at 3 months induction. G, H: Typical cell loss in the same region at 9 months induction. Note in A-H, rTG4510(-) images are on the left and data from (+) littermates on the right. I: Typical synapses in the DG ML (red arrows indicate post-synoptic densities: PSDs). J: Mean DG ML DG PSD length, pre-synaptic vesicular pool area and pre-synaptic vesicle density (vesicle number/pool area) in rTG4510 (-) and (+) littermates at 1 and 3 months induction. No significant differences are apparent. K: Examples of myelinated axon cross-sections in DG ML showing diameter (calculated from area) and g-ratio following 1 month induction. L: G-ratio across the diameter range at 1 month induction in both sets of littermates; mean difference on the right showing significantly higher g-ratio following mutant tau induction. “n” numbers refer to the number of individual synapses or axons examined; mean data collected from a minimum of 4 grid sections from at least two different mice. Scale = 10 μm (A-H), 100 nm (I), 500nm (K).

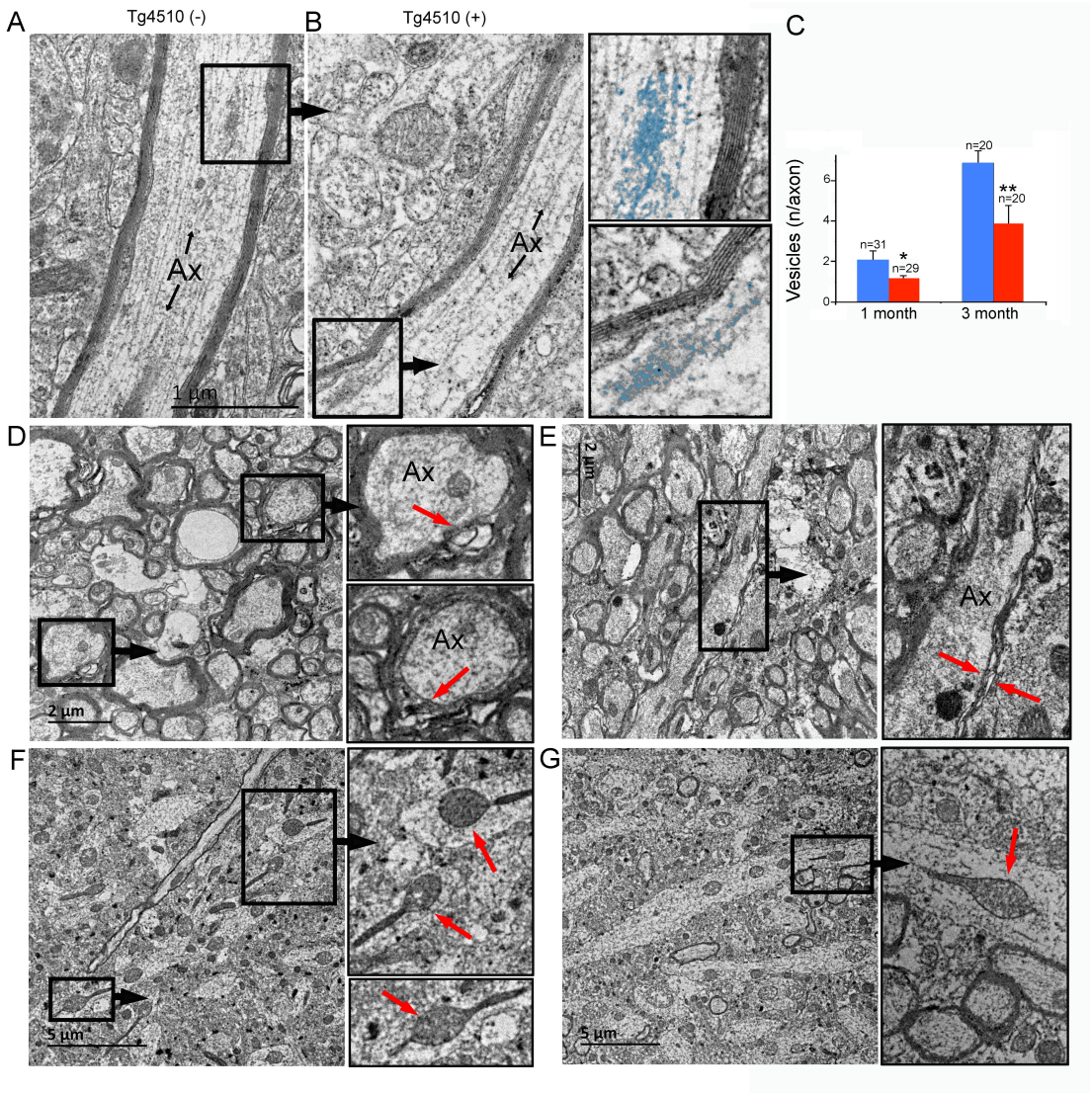

Figure 2. Myelinated axon pathology following mutant tau induction. A-C: Axoplasmic vesicle density in myelinated axons at 1 and 3 months induction in rTG4510(-) and (+) littermates. Examples of vesicle clusters are shown in longitudinally oriented ML DG axons ("Ax") (A, B), with the boxed areas shown at higher gain to the right (vesicle shaded blue). D, E: Typical myelinated axon pathology in the CA2 paraventricular alveus in rTG4510(+) mice at 1 month induction. Note myelin ad-axonal myelin separation and sub-myelinic lacunae (red arrows in boxed area to the right) evident in axons sectioned in X-S (D) and L-S (E). F: Typical features of CA2 stratum oriens adjacent to alveus in the same animal. Note the normal myelinated axon morphology and the presence of numerous "MOAS"-mitochondria (red arrows). G: Similar region in a rTG4510 (-) littermate. Note the normal myelinated axon profiles and the single "MOAS"-mitochondria (red arrow). "n" numbers refer to the number of individual axons examined; mean data collected from a minimum of 4 grid sections taken from at least three different mice.

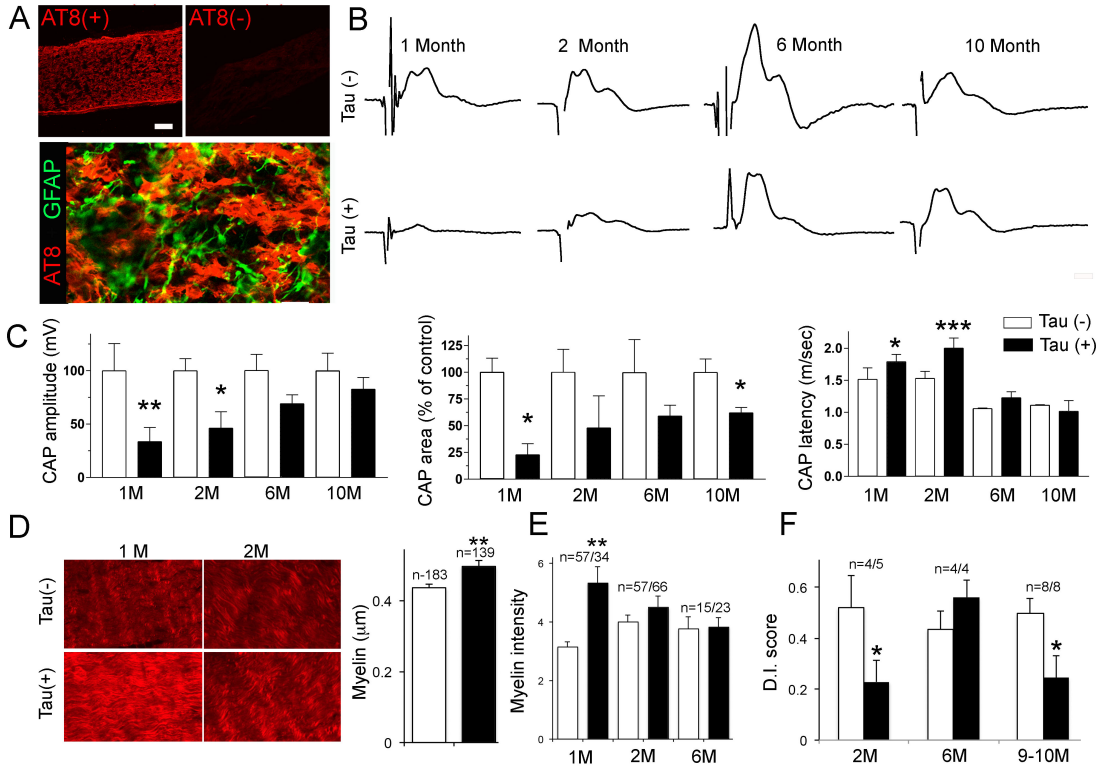

Figure 3. Mutant tau induction evoked rapid transient failure of WM function and simultaneous memory decline. A: Tau hyper-phosphorylation detected with AT8 reactivity in ON (top left), omission of primary antibody yields no staining (top right). Co-staining with GFAP showed tau hyper-phosphorylation in neighboring axons (red) but not in the astrocytes (green) (bottom). B: Representative CAPs recorded from ONs after various periods of doxycycline withdrawal in tau (-) (top) and (+) (bottom) rTG4510 littermates. C: Electrophysiological parameters at the four age points, showing significant loss of CAP amplitude and area and an increase in conduction latency after 1-2 months of transgene induction that normalized after 6-10 months induction (n=4 nerves in all cases). In this and subsequent figures open bars = rTg4510(-) and filled bars = rTg4510(+). D (left): FM-red myelin staining at 1 and 2 month induction. D (right): The width of FM-Red stained myelin sheaths after 1 month induction. Note the significant increase in rTG4510(+) compared to littermates, (n = myelin sheaths mesured from a minimum of three animals). E: FM-red myelin staining intensity at 1, 2 and 6 months induction (n= number of regions). F: Novel recognition test performance (D.I. score) at 2, 6 and 9-10 months induction in rTG4510(-) and (+) littermates (n=number of mice).

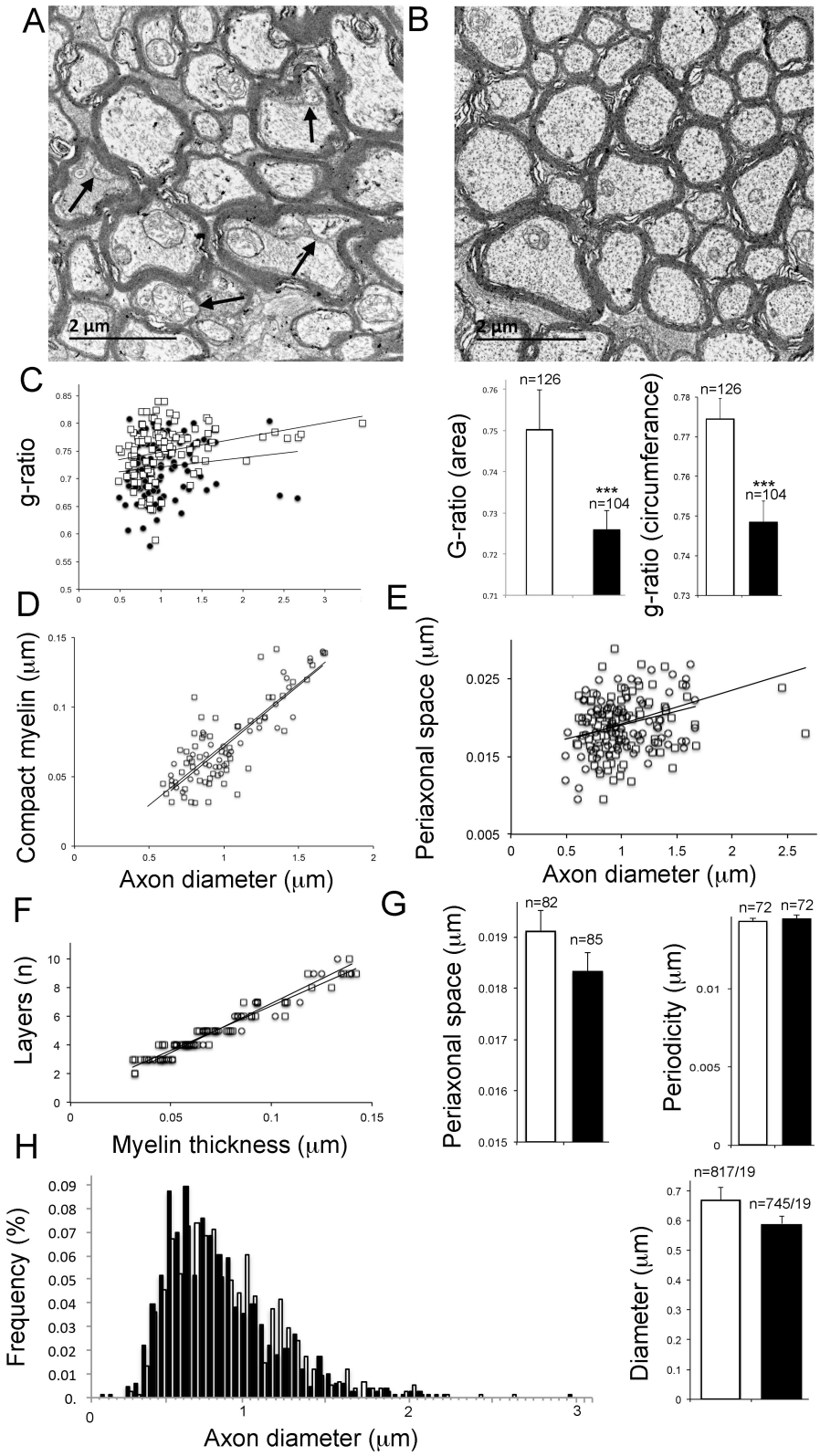

Figure 4. Myelin structural parameters at 1 month mutant tau induction in ON. A, B: X-S ultra-micrographs in rTG4510 (+) (A) and rTG4510 (-) (B) ON. Examples of ad-axonal myelin pathology are indicated by arrows. C: G-ratio across the axon diameter spectrum following transgene induction measured using ideal diameter calculated from axon area. The mean g-ratio calculated in this way or from the measured circumference is shown to the right. D, E:

The width of compact myelin and the periaxonal space was not affected by transgene induction at any axon diameter. F: The relationship between the number of myelin layers and axon diameter was not affected by tau induction. G: Mean myelin periodicity and periaxonal space width were not significantly affected by transgene induction. H: Axon diameter distribution (left) and mean axon diameter (right) were also unaffected. Open bars = rTg4510(-) and filled bars = rTg4510(+), n = number of axons measured (C, E, G) or axons measured/sections (H); data collected from a minimum of three mice per mean.

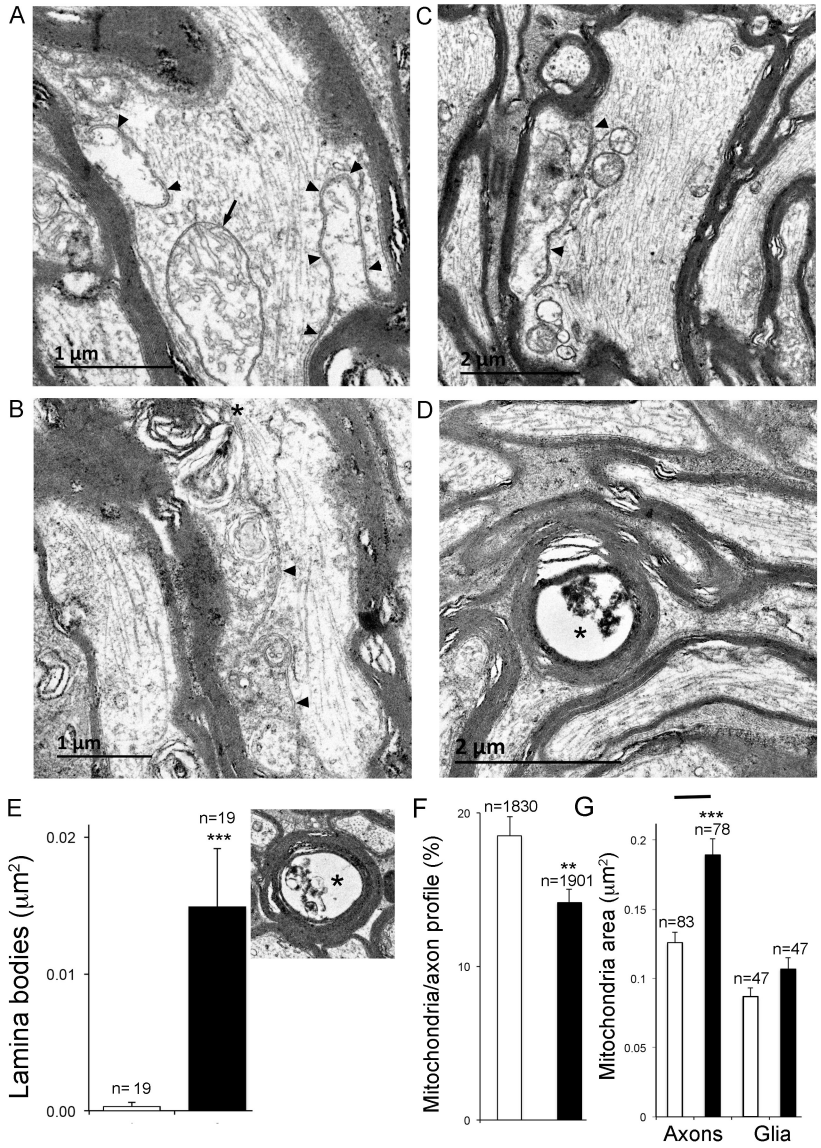

Figure 5. Structural defects in the ad-axonal face of the myelin sheath following mutant tau induction in the ON. A-E: L-S ultra-micrographs showing the range of severity of focal defects in tau(+) rTG4510 RON at 1 month induction. Note the infolding of the axolemma (arrow heads), and the associated focal myelin decompaction and blebbing (e.g., asterisks). Mitochondria (arrow) have a normal appearance. Myelin occasionally formed axoplasmic lamina bodies containing large vacuoles (D) which in X-S have the appearance of dystrophic axons (E). E: The density of large lamina bodies in X-S is significantly higher in rTG4510 (+) littermates. F: The proportion of axons in X-S containing mitochondrial profiles. G: Mitochondrial volume is significantly larger following transgene induction in axons but not glia. Open bars = rTg4510(-) and filled bars = rTg4510(+), n = number of axons or glial cells; data collected from a minimum of three mice per mean.

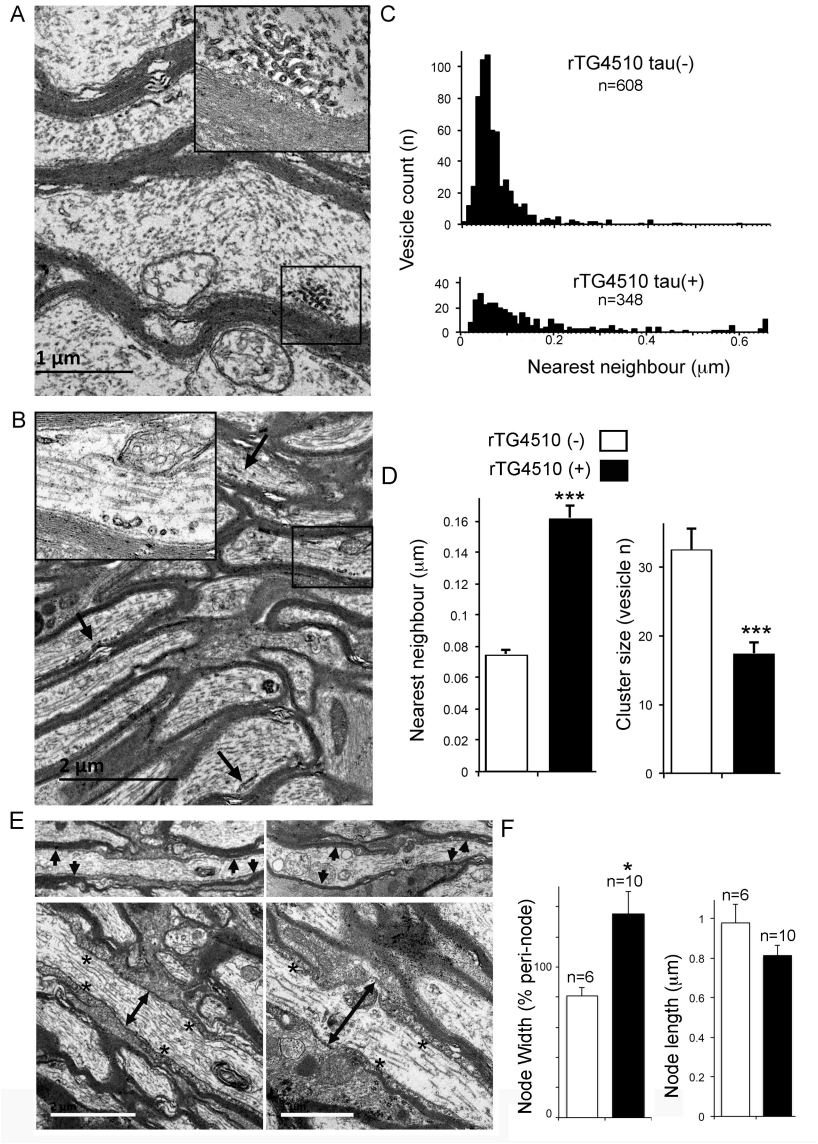

Figure 6. Axoplasmic vesicle distribution is altered at 1 month of mutant tau induction in the ON. A: Sub-myelinic clusters of 20-40 nm axon vesicles are apparent in tau (-) rTG4510 RON axons, often incorporating occasional cylindrical profiles (boxed area shown at higher gain). B: Vesicle clusters were less focal and contained fewer elements in tau (+) littermates. Several clusters indicated by the arrows with the boxed example shown at higher gain. C, D: Nearest-neighbor analysis of axon vesicles and mean cluster size, confirming this observation. E: Typical nodes of Ranvier showing enlarged nodal diameter in tau(+) littermates (right) compared to (-) littermates (left). (paranodal end-loop regions indicated by "*"). Lower power images are shown at the top to demonstrate the compact myelin in internodal regions either side of the myelin-free nodes (e.g., short arrows). F: Analysis of node width at the widest point relative to the peri-nodal axon width, and nodal length. Open bars = rTg4510(-) and filled bars = rTg4510(+), bars = 1 µm (E), n = number of vesicle or nodes; data collected from a minimum of three mice per mean.

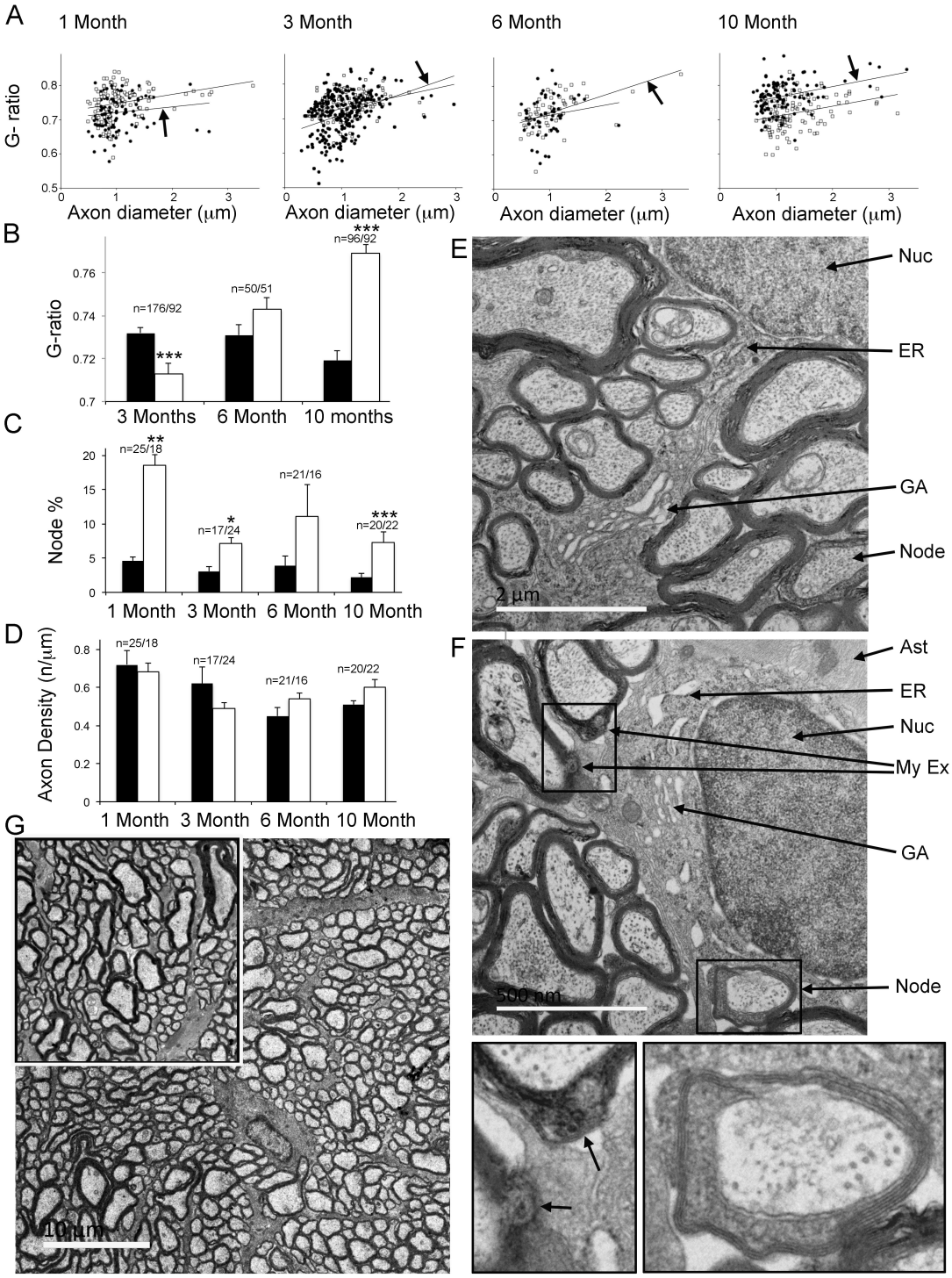

Figure 7. Myelin remodeling without demyelination in the ON. A: G-ratio at 4 time periods of mutant tau induction (filled symbols) compared to tau(-) littermates (open symbols). The linear regression lines for tau(+) littermates are indicated by the arrows. Note that myelin expansion is gradually replaced by myelin thinning across the diameter range. B: Mean G-ratio at older time points. C: The proportion of node of Ranvier profiles relative to internodal myelin profiles in X-S is significantly elevated across the age spectrum. D: Mean myelinated axon density is not significantly different in any age-group. E, F: Structural characteristics of tau(-) (E) and tau(+) oligodendrocytes at 10 months transgene induction. Note the homogeneous chromatin in the nucleus

(“Nuc”), the expanded endoplasmic reticulum (“ER) in “F”, the normal Golgi apparatus (“GA”) and Node of Ranvier (“Node”) in both cases. Focal regions of myelin expansion (“My Ex”) are apparent in “F”. Boxed areas shown at higher magnification below. G: Low-power images of tau(+)axons and glia at 10 months induction (tau(-) shown in the insert for comparison). Open bars = rTg4510(-) and filled bars = rTg4510(+), n = number of axons; data collected from a minimum of three mice per mean..

.

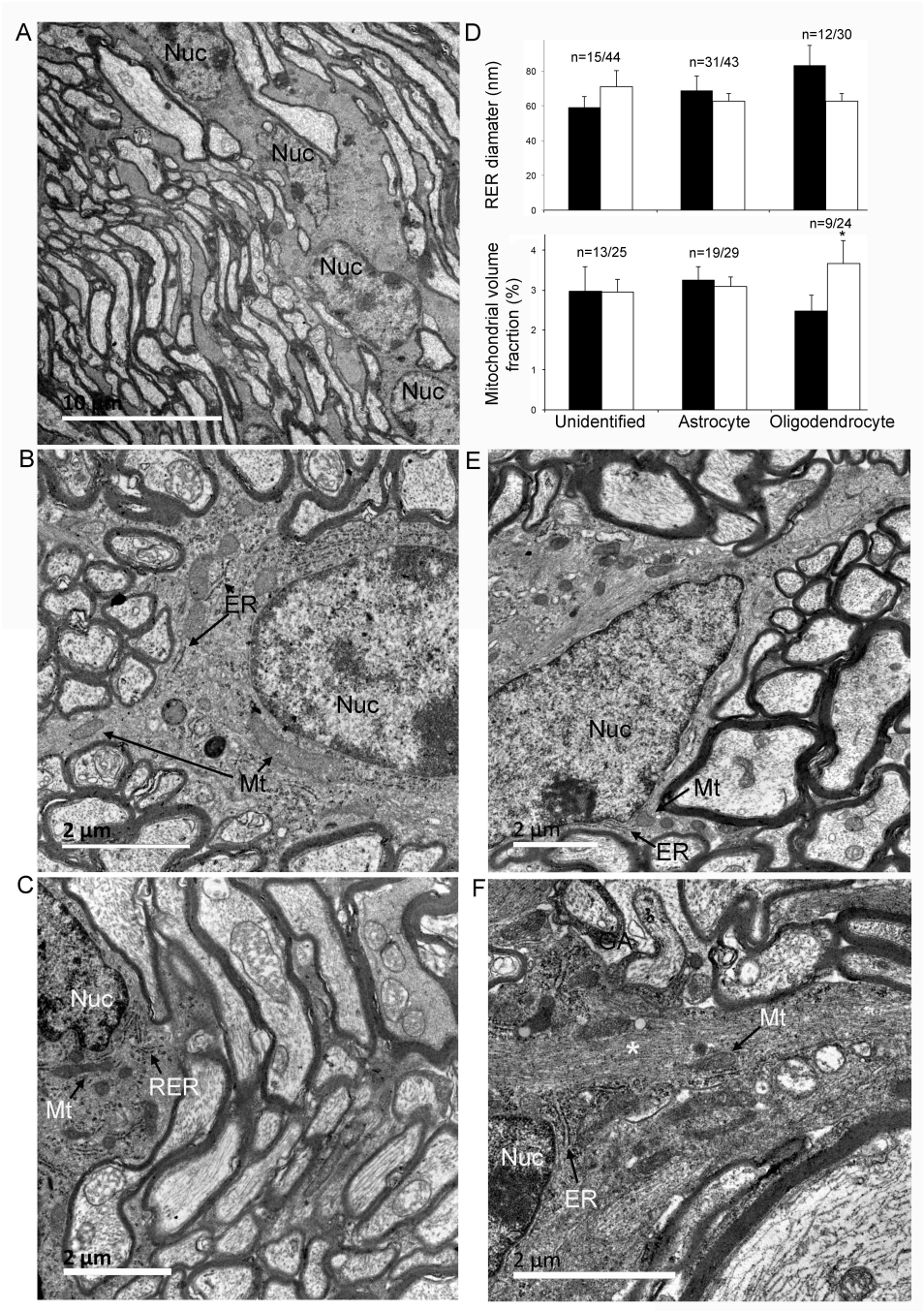

Figure 8. Changes to ON glial cells are limited. A: A chain of typical oligodendrocyte somata running parallel to axons following 1 month transgene induction shown in L-S. B: The nucleus ("Nuc"), endoplasmic reticulum ("ER") and mitochondria ("Mt") exhibit normal structure (X-S, 1 month induction). C: Astrocyte showing no features of reactive changes (L-S, 1 month). D: Rough ER ("RER") diameter is not significantly different in unidentified glia, astrocytes or oligodendrocytes following 3 months induction. Mitochondrial volume fraction shows a small elevation in oligodendrocytes (n= cell number). E, F: Typical oligodendrocyte (E) and astrocyte (F) in X-S at 6 months induction, "*" = glial filaments. Scale = 2 μm in all cases. Open bars = rTg4510(-) and filled bars = rTg4510(+), n = number of axons; data collected from a minimum of three mice per mean.

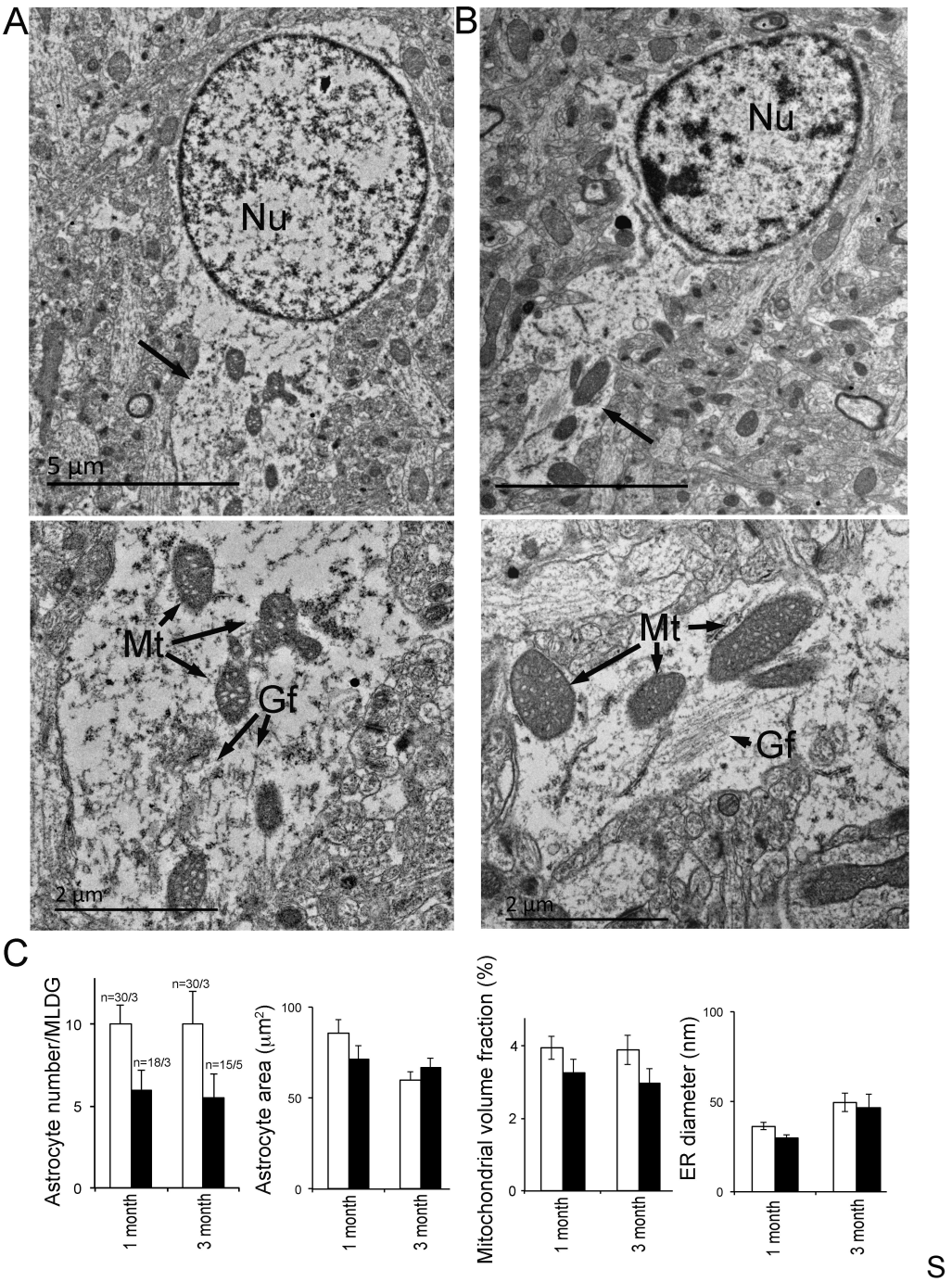

S

Figure S 1. No structural changes in dentate gyrus astrocytes following mutant tau induction. A, B: ML astrocytes after 1 month (A) and 3 months (B) mutant tau induction. Lower power ultramicrographs are shown on the top with the major process shown at higher gain below ("Nu" indicates the nuclei). Note the normal appearance of the mitochondria ("Mt") and the presence of glial filaments (Gf) which positively identify the cells as astrocytes. C: All astrocytes identified on structural grounds within a single plane section were counted in 3 tau(-) and 3 tau(+) mice showing no significant difference in the number of astrocytes following mutant tau induction. There was no significant difference in the area of these cells, their mitochondrial volume fraction or their endoplasmic reticulum (ER) diameter; n = number of astrocytes/ number of mice (same for all histograms).

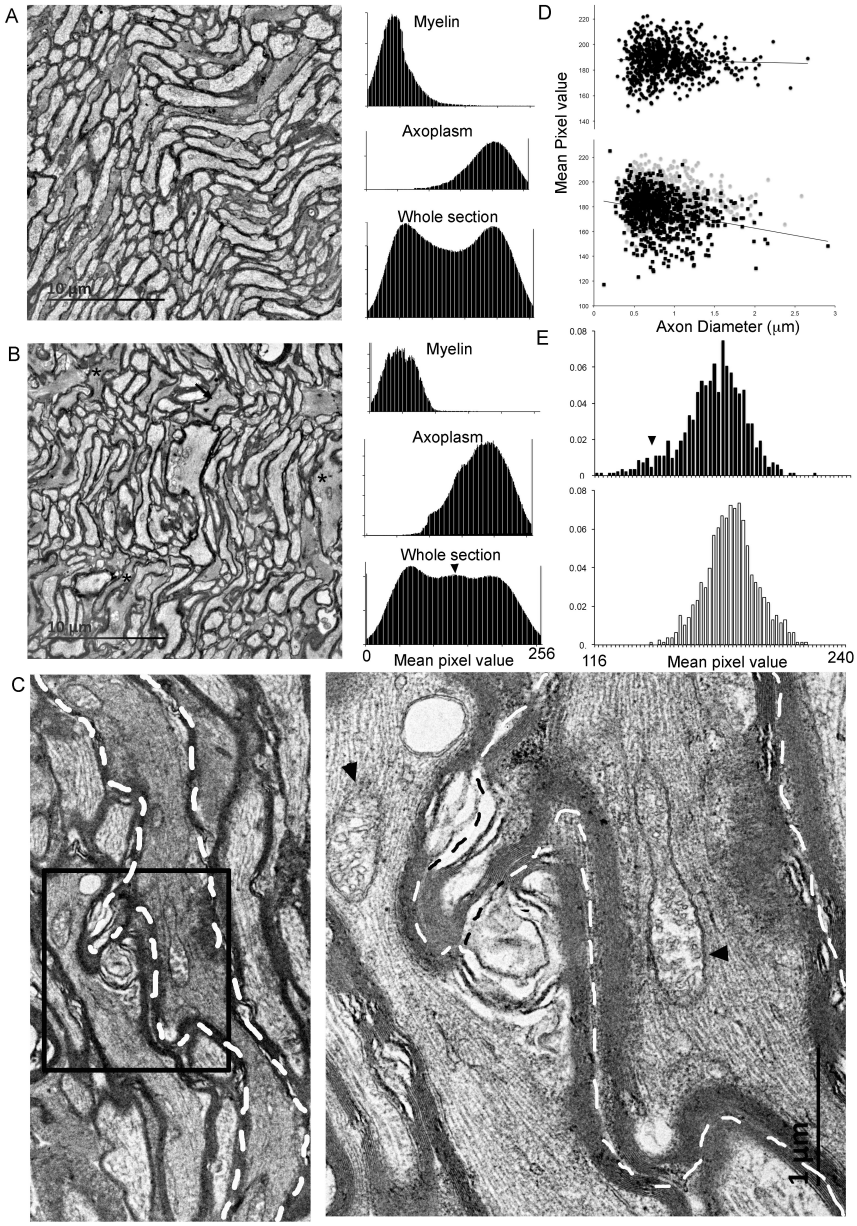

Figure S 2. Dark axons. A: Low power L-S ultra-micrograph showing numerous ON myelinated axons (left) and the pixel intensity profiles of the component myelin, axoplasm and the whole image (right). Note that low intensity indicates darker shades (i.e., to the left) and that the whole profile incorporates clear myelin and axoplasm peaks. B: Similar analysis taken from tau(+) littermate, showing the presence of dark axons (left: asterisks). Note the presence of a darker component to the axoplasm and whole section intensity profiles (arrow head) correlating with dark axoplasm. C: Higher gain image showing a dark axon with a normal mitochondria (arrow head) and sub-myelinic blebbing (boxed area shown at higher gain to the right). D: Pixel intensity was uniform in axons of different diameters in tau(-) littermates (top), but was significantly darker in particular within larger axons in tau(+) littermates (bottom, control data shown gray for comparison). E: Axon intensity distribution, showing a population of dark axons in tau (+) littermates (n=600 axons) (top) compared to tau (-) (n = 450 axons)(bottom).

Acknowledgments: We thank Waldemar Woznica for assistance with animal care. This work was supported by BBSRC (J016969/1), Alzheimer's Research UK (South-West network centre grant), and by the University of Plymouth.

Competing interests: none.

Author contributions: AD performed and analyzed CAP recordings and contributed to colony management; JJ, GB and RF performed and analyzed the EM; KC performed and analyzed the behavioral test; PB prepared the EM samples; OA managed the transgenic colonies and contributed to study design; RF supervised and designed the project, developed the ideas and wrote the manuscript.